Ultrasonics Sonochemistry 83 (2022) 105928

Contents lists available at ScienceDirect

Ultrasonics Sonochemistry

journal homepage: www.elsevier.com/locate/ultson

Pickering emulsion prepared by nano-silica particles – A comparative study for exploring the effect of various mechanical methods

Jixuan Gao [a], Xiangning Bu [a,*], Shaoqi Zhou [a], Xuexia Wang [a], Muhammad Bilal [b], Fawad Ul Hassan [b], Ahmad Hassanzadeh [c,d], Guangyuan Xie [a], Saeed Chehreh Chelgani [e]

[a] Key Laboratory of Coal Processing and Efficient Utilization (Ministry of Education), School of Chemical Engineering and Technology, China University of Mining and Technology, Xuzhou 221116, China
[b] Department of Mining Engineering, Balochistan University of Information Technology, Engineering and Management Sciences (BUITEMS), Quetta, Pakistan
[c] Department of Geoscience and Petroleum, Faculty of Engineering, Norwegian University of Science and Technology, 7491 Trondheim, Norway
[d] Maelgwyn Mineral Services Ltd, Ty Maelgwyn, 1A Gower Road, Cathays, Cardiff CF24 4PA, United Kingdom
[e] Minerals and Metallurgical Engineering, Dept. of Civil, Environmental and Natural Resources Engineering, Luleå University of Technology, SE-971 87 Luleå, Sweden

ARTICLE INFO

Keywords:
Pickering emulsion
Nano-silica
Rotor–stator homogenization
Ultrasound emulsification

ABSTRACT

Pickering emulsions are eco-friendly, stabilized by solid particles, and have an essential role in leading industries. Although Pickering emulations have found several applications, surprisingly few investigations have attempted to explore the effectiveness of various mechanical processes for its production. To fill these gaps, the present investigation comprehensively examined the application of various Pickering emulsion preparation processes such as rotor-stator homogenization emulsification (R-SH), ultrasonic emulsification, and their combined processes by using nano-silica particles. The influences of emulsification time and intensity on emulsion droplets' distribution were analyzed as indicative factors. The kerosene/water nano-silica Pickering emulsion was utilized for all assessments. The obtained results demonstrated that the main distribution peak of the emulsion prepared by R-SH occurred where the chord length was greater than 40 μm. Micro-scale nano-silica-aggregates generated large droplets, while the fine-emulsion fraction was significantly increased after ultrasonic treatment. The experimental results showed that the emulsion prepared only by ultrasound needed substantial power to form a Pickering emulsion since the oil phase was difficult to disperse in the water phase. Finally, it was concluded that preprocessing by R-SH could form a stable and uniform emulsion speedily, which is essential for ultrasound emulsion preparation.

1. Introduction

Pickering emulsions are the type of emulsions that are typically stabilized by solid particles instead of surfactants [1–3]. Compared to traditional surfactant-stabilized emulsions, Pickering emulsion has several potential advantages: low cost and reduced emulsifier consumption, eco-friendliness and low toxicity to the human body, strong stabilization, and no susceptibility to factors such as pH, salt concentration, temperature, and oil phase composition [4]. Hence, this emulsion has vital applications in food, cosmetics, medicine, mining, and other industries. Further, a variety of solid particles can be used for stabilization, including clays [5], carbon black [6], polysaccharide [7], and inorganic particles [8]. The effectiveness of the solid stabilizing emulsions depends on multiple factors; among them, the most important one is related to the particles having a certain degree of wettability. The size of particles should also be finer than the emulsion droplet, at least by order of magnitude [9].

In recent years, with the development of nanotechnology, various nanoparticles were synthesized whose application for Pickering emulsion stabilization led to significant enhancement in their production process. Binks discussed the preparation process and properties of oil-in-water emulsions stabilized by colloidal silica particles, focusing on the effect of particles' wettability and proportion [3]. After that, the effect of oil–water ratio on emulsions properties was reported in other investigations [2,3,9–11]. Whitby et al. explored the properties of such emulsions formed in the presence of colloidal mixtures of hydrophobic titania and hydrophilic silica particles. They indicated that the silica particles were not attached to the droplets' surface and did not form a

* Corresponding author.
E-mail address: xiangning.bu@cumt.edu.cn (X. Bu).

https://doi.org/10.1016/j.ultsonch.2022.105928
Received 20 August 2021; Received in revised form 13 January 2022; Accepted 18 January 2022
Available online 21 January 2022

Table 1
Characteristics of different emulsification technologies [18]. (+ = yes; - = no; +/- = intermediate).

Methods	Easy setting-up	Quick process	Absence of particle disruption risk	Absence of temperature rise risk	Possibility to obtain sub micrometric droplets	Low poly disparity	Low energy consumption	Potential industrialization
Rotor-stator homogenization	+	+	–	–	–	–	+/-	+
Ultrasonic	+	+	–	–	+	–	+/-	–
Membrane	–	–	+	+	+	+	+	–
Microfluidic	–	–	+	+	+	+	+	–

particle layer like the titania particles. Nevertheless, the concentration of silica particles affected the stability of the emulsion [12]. It was reported that the stabilization of emulsions by two types of particles (i.e., bentonite and magnesium aluminum hydroxide) with opposite charges makes the emulsions reasonably stable. It was also demonstrated that the flow behavior of the emulsion was dependent on the mass fraction of the hydroxide. Also, the emulsion stability was not affected by the mixing ratio of the two compounds when the total solid content was 0.5% [13]. However, only a few studies explored the effect of mechanical processes on Pickering emulsion production.

Pickering emulsion can be prepared using different mechanical processes, including rotor–stator homogenization (R-SH), ultrasonic, and membrane emulsification, as well as microfluidic technology [4,14-17]. These methods have various advantages based on the applied technologies (Table 1). For instance, the R-SH is one of the most commonly employed techniques. Its marked advantages (i.e., simplicity, convenience, and low cost) make it a suitable method for industrial-scale production. Still, it has one drawback, i.e., the emulsion made by this method may not be uniform due to the limit of energy input.

In recent years, the ultrasound method has also been frequently used for the emulsification process [19]. Compared with the R-SH, ultrasound has higher energy input. The violent cavitation and shear stress caused by ultrasound can promote the adsorption of a stabilizer on the two-phase interface [4]. Besides, the droplet size of the emulsion is smaller, and the stability is higher [20,21]. However, it also has some limitations. The violent collapse of ultrasonic cavitation bubbles primarily leads to a sharp temperature enhancement, resulting in a high energy cost [4]. Other methods like membrane emulsification and microfluidic technology are low energy-intensive and environmentally friendly. In the membrane emulsification process, the liquid phase is forced through the membrane pores, forming droplets on the penetration side of the membrane, and then the droplets are carried away [22]. Microfluidic technology, such as membrane emulsification, is a drop-by-drop technology. The major limitation of membrane emulsification and microfluidic technology is the low yield [16].

Although the influence of particle properties on emulsion stabilization has been widely examined, little attention has been paid to the mechanical processes for producing Pickering emulsions. This study is aimed to explore the effect of two traditional mechanical processes (R-SH and ultrasound) on the characteristics of Pickering emulsion stabilized by nano-silica particles (NSP). The emulsification time of both traditional mechanical processes on the emulsion features is investigated. Afterward, a proper combination of these two mechanical processes is presented. Finally, the properties of emulsions (emulsion droplet size and distribution) prepared by different mechanical methods are compared based on the optimal technique.

2. Experimental process

2.1. Materials

Kerosene was used as the emulsion's oil phase (Sinopharm Group Co. Ltd., China). Kerosene emulsion is commonly used as a collector for graphite's flotation processes [23,24] and coal [25,26]. Therefore, kerosene was still chosen for further research on kerosene Pickering emulsion. Deionized water was used as the water phase (DI; resistivity 18.2 MΩ•cm) and nano-silica particles (NSP) (20 ± 0.5 nm) (LABCOM laboratory Supplies Mall (Beijing, China)), Cyclohexane (Xilong Chemical Co., Ltd.), and trimethylchlorosilane (Sinopharm Chemical Reagent Co., Ltd.) were used for the hydrophobic modification of NSP.

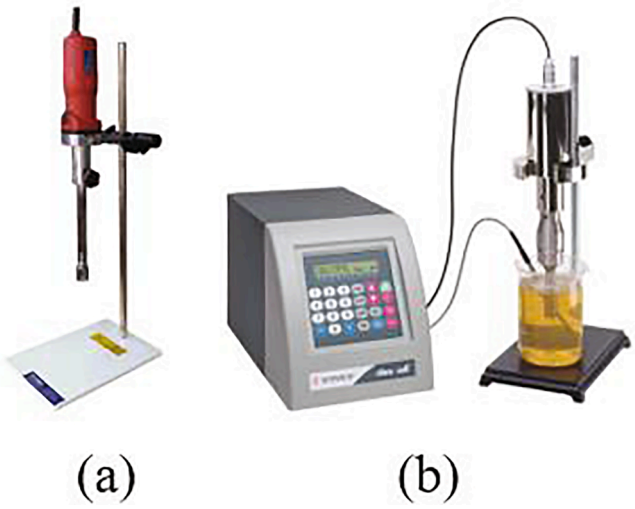

Fig. 1. A schematic demonstration of the high-speed homogenizer (a) and ultrasound device (b) for emulsification.

2.2. Hydrophobic modification of NSP

It is well documented that particles with good hydrophilic or hydrophobic properties are not conducive to the stability of emulsions [27,28]. Thus, a hydrophobic NSP was prepared, and the modification process was performed in a 250 mL Erlenmeyer flask. 2.5 g NSP was dispersed into the trimethylchlorosilane (150 μL) diluted with Cyclohexane (100 mL) at room temperature. The chemical reaction took >12 h to complete. Once the reaction was completed, the NSP was separated from solutions by drying at 80 ℃ temperature. The reaction during the process is expressed as follows [29]:

$$-\mathrm{Si}-\mathrm{OH}+(\mathrm{CH_3})_3\mathrm{SiCl}\rightarrow-\mathrm{Si}-\mathrm{O}-\mathrm{Si}(\mathrm{CH_3})_3+\mathrm{HCl} \quad (1)$$

2.3. Emulsion preparation

The amount and size of added NSP affect the emulsion properties [2,30,31], which were kept constant in this work. However, the effect of different emulsification methods on the emulsion is the main target of this investigation. Before the emulsification process, the hydrophobic NSP (0.20% w/w) was pre-dispersed in oil. In each given emulsification test, 50 mL emulsion was prepared with a fixed oil–water ratio (20%). The high-speed homogenizer (FLUKO Shanghai Equipment Co., Ltd, China) was used for R-SH (Fig. 1a). A 20 kHz ultrasound device (VCX 800, SONICS, US), having 800 W power, was used for ultrasonic emulsification (Fig. 1b). This ultrasound device changes the magnitude of

Table 2
The experimental parameters and levels for different preparation methods.

Preparation method	Parameter	Level
R-SH	Intensity (Stirring speed, rpm)	10000, 13000, 16000, 19,000
	Time (min)	1, 2, 4, 6, 8, 12
Ultrasound	Intensity (%)	20, 50, 80
	Time (min)	6, 10, 20
Combined R-SH with ultrasound	Ultrasound intensity (%)	20, 30, 40, 50, 60, 80, 100
	Ultrasound time (min)	1, 2, 4, 6, 8
	R-SH time (min)	1, 2, 4, 6, 8

ultrasound energy input by varying the ultrasound amplitude. In this study, the ultrasound intensity refers to the percent of ultrasound amplitude. The experimental parameters and levels are given in Table 2. The oil-in-water emulsion was prepared thrice. After the emulsion was prepared, the droplet distribution and optical microscopic images of each emulsion were immediately measured to describe their properties.

2.4. Measurement of the emulsion properties

2.4.1. Characterization of Pickering emulsion droplets distribution

The droplet size distribution measurements were carried out using focused beam reflectance measurement G400 (FBRM) (Mettler-Toledo Ltd., Redmond, WA, USA). FBRM probe was put into 1 mL of emulsion diluted into 300 mL ultrapure water being stirred at 450 rpm during the measurement. The chord length distribution of the emulsion droplet size was thus obtained. When the particle passes through the measurement area, the focused beam hits one side of the particle and is reflected. At this time, the enhanced signal continues to be detected until it reaches the other side of the particle. The time of this reflected beam is multiplied by the scanning speed to get the distance, so-called the particle's "chord length". The microscopic morphology of the emulsion was obtained by polarizing microscopy (Sunny Optical-Instrument, Zhejiang, China) at a magnification of 20x. A small amount of emulsion taken by the straw was applied to the glass slide, and optical microscopic images of emulsion droplets were obtained.

FBRM and optical microscopic images provide qualitative and quantitative estimations of the droplet size. The emulsion results were analyzed for the mean droplet diameter (d_{50}), Sauter mean diameter ($D_{3,2}$) presented in Eq. (2)., volume mean diameter ($D_{4,3}$) as shown in Eq. (3), and relative span (δ) [38] given in Eq. (4).

$$D_{3,2} = \frac{\sum(nd^3)}{\sum(nd^2)} \tag{2}$$

$$D_{4,3} = \frac{\sum(nd^4)}{\sum(nd^3)} \tag{3}$$

where n is the number of particles with diameter d.

$$\delta = \frac{d_{90} - d_{10}}{d_{50}} \tag{4}$$

where d_{90}, d_{10}, d_{50} are the droplet diameters corresponding to 90%, 10% and 50% (v/v) on accumulation curve. δ is used to characterize the emulsion dispersion; <0.5 indicates a higher degree of monodispersity.

Relative standard deviation (RSD) was used to describe the reliability of the experimental data:

$$\mathrm{RSD} = \frac{\mathrm{S}}{\bar{\mathrm{x}}} \times 100\% \tag{2}$$

where S is the standard deviation; $\bar{x}$ is the average. RSDs are shown in Table A1 to Table A6 (in the appendix). Interestingly, the measurement size indicated by FBRM varied from that indicated by the optical microscope images under the same conditions. Similar phenomena have been reported by other investigations [32-35]. FBRM results are compared with alternative particle sizing techniques such as laser diffraction, ultrasonic attenuation spectroscopy, image analysis, and sieving analysis [32-36]. A lot of literature [32-36] has reported the phenomena that the FBRM oversized fine particles and undersized coarse ones compared to other particle sizing techniques. Some RSD values >5% were observed in the appendix, which may be attributed to the inherent flaws of the FBRM technique. It is notable that the literature also shows strong linear relations for measurement results between

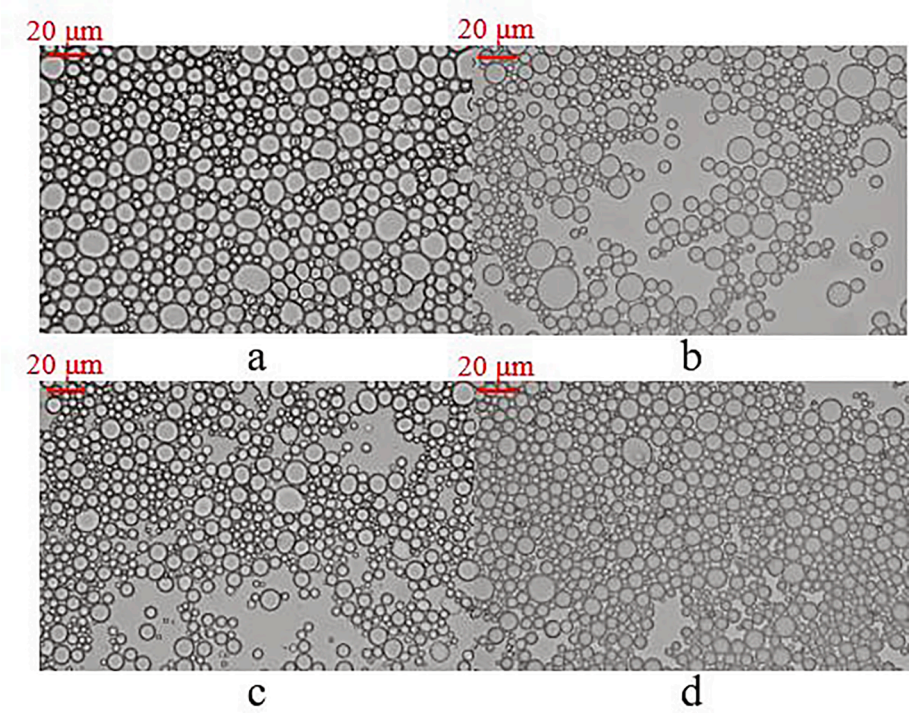

Fig. 2. Optical microscopic images of emulsion droplets prepared by R-SH with different intensities: (a) 10,000, (b) 13,000, (c) 16,000, and (d) 19,000 rpm.

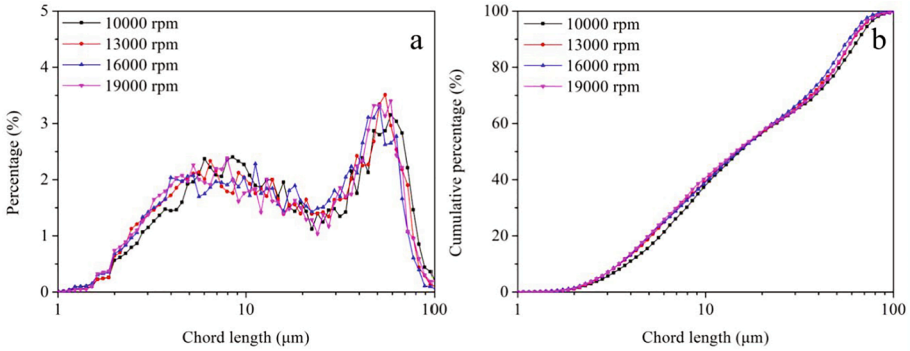

Fig. 3. Chord length of emulsion droplets prepared by R-SH with different intensities (a is distribution curve, and b is accumulation curve).

Table 3
d_{10}, d_{50}, d_{90}, $D_{3,2}$, $D_{4,3}$, and δ of emulsion droplets prepared by R-SH with different intensities.

Average diameter	R-SH intensity (rpm)			
	10,000	13,000	16,000	19,000
d_{10} (μm)	3.86 (±0.35) [3.28,4.20]	3.48 (±0.19) [3.29,3.73]	3.48 (±0.09) [3.35,3.56]	3.45 (±0.09) [3.35,3.53]
d_{50} (μm)	15.50 (±1.13) [14.05,16.69]	14.86 (±1.41) [13.33,17.12]	14.63 (±1.03) [13.71,15.82]	14.49 (±0.53) [13.81,15.17]
d_{90} (μm)	65.35 (±1.60) [62.94,67.09]	60.78 (±1.17) [58.96,61.90]	58.09 (±2.41) [54.73,60.24]	61.04 (±0.85) [60.01,62.03]
$D_{3,2}$ (μm)	61.49 (±1.39) [60.25,63.63]	57.55 (±1.67) [55.12,59.35]	55.00 (±2.37) [50.96,56.77]	58.08 (±0.97) [56.48,59.11]
$D_{4,3}$ (μm)	68.24 (±2.04) [66.75,71.59]	63.88 (±2.01) [61.15,65.91]	61.47 (±2.78) [56.53,63.22]	64.67 (±1.41) [62.47,66.31]
δ	3.98 (±0.23) [3.77,4.24]	3.88 (±0.32) [3.33,4.16]	3.75 (±0.34) [3.27,4.10]	3.97 (±0.17) [3.73,4.16]

Note: $[a_1,a_2]$—a_1 and a_2 are the minimum and maximum values of the measured data.

FBRM and other particle sizing techniques [32-37]. Most of the RSDs in the appendix are smaller than 5%, which supports the availability of the FBRM. Thus, the FBRM is a reliable particle sizing technique.

2.4.1.1. NSP size measurement. The size of the NSP was measured using Nano Brook Omni (Brookhaven, US). 0.20 g of NSP was dispersed in 50 mL ultrapure water, and 1 mL solution was used for size measurement. Measurement was repeated five times, and the average was reported as the final value.

2.4.1.2. Zeta potential of NSP. The zeta potential of the NSP was measured using Nano Brook Omni (Brookhaven, US). Disperse 0.20 g of NSP in 50 mL ultrapure water, and 1 mL solution was used for the test. Each experiment was repeated five times, and the average was considered as the final value.

2.4.1.3. NSP X-ray photoelectron spectroscopy. To observe the influence of R-SH or ultrasonic on the NSP surface, XPS was used to analyze the NSP surface. The model of XPS used in the test is ESCALAB 250xi (Thermo Fisher, USA). XPSPEAK41 fitted the obtained data. Physical displacement was produced in the process of testing non-conductive samples, and the degree of displacement was different according to

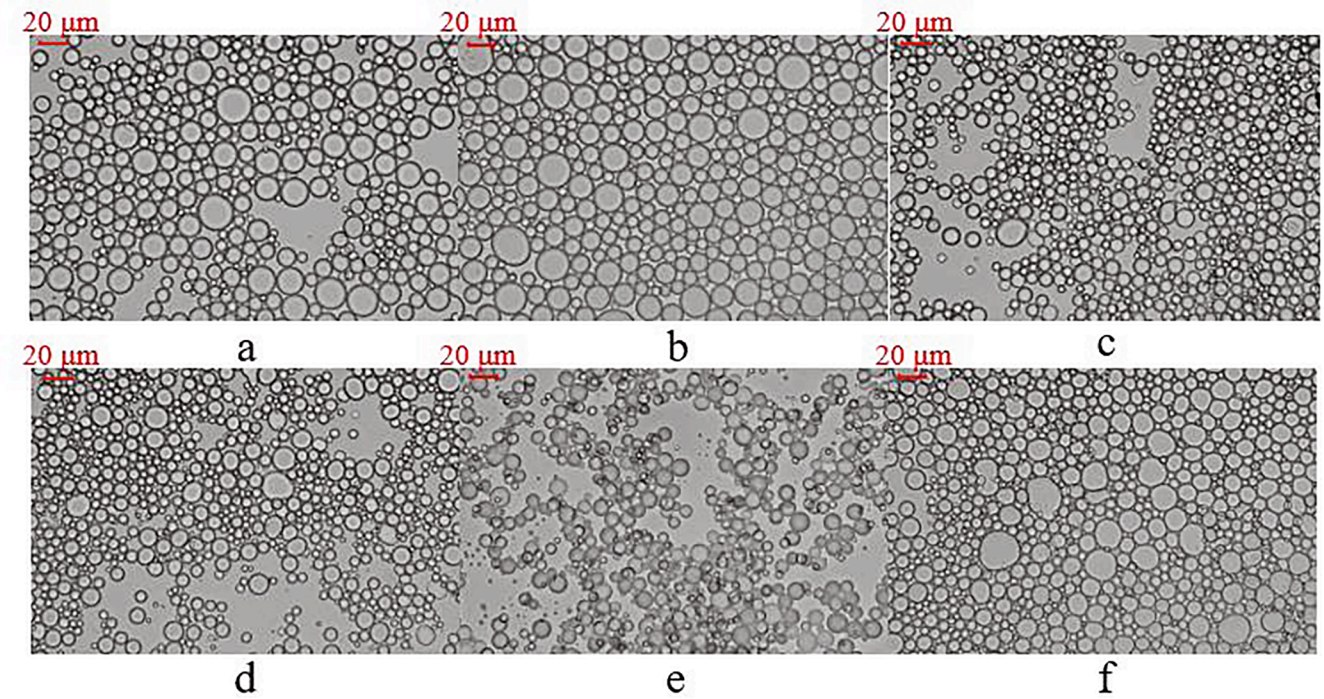

Fig. 4. Photographic images of emulsion droplets prepared by R-SH at different times: (a) 1, (b) 2, (c) 4, (d) 6, (e) 8, and (f) 12 min.

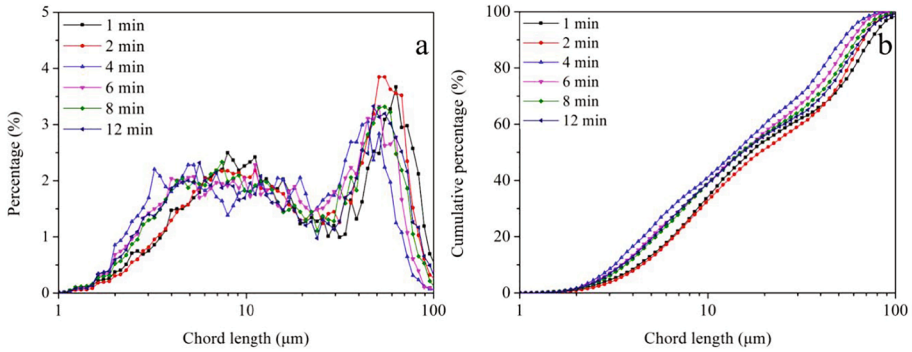

Fig. 5. Chord length of emulsion droplets prepared by R-SH at different times (a is distribution curve, and b is accumulation curve).

Table 4
d_{10}, d_{50}, d_{90}, $D_{3,2}$, $D_{4,3}$, and δ of emulsion droplets prepared by R-SH at different times.

Average diameter	Time (min)					
	1	2	4	6	8	12
d_{10} (μm)	4.28 (±0.46) [3.80,5.03]	4.28 (±0.56) [3.34,4.69]	3.20 (±0.15) [3.05,3.35]	3.48 (±0.09) [3.35,3.56]	3.65 (±0.23) [3.32,3.89]	3.47 (±0.14) [3.31,3.64]
d_{50} (μm)	16.53 (±1.35) [15.06,18.62]	17.78 (±2.11) [14.32,19.49]	13.76 (±0.67) [13.00,14.53]	14.63 (±1.03) [13.71,15.82]	15.05 (±1.07) [13.41,16.27]	15.37 (±0.85) [14.27,16.63]
d_{90} (μm)	73.77 (±2.09) [70.79,75.55]	64.61 (±5.82) [54.25,67.13]	52.46 (±1.15) [51.62,54.28]	58.09 (±2.41) [54.73,60.24]	62.41 (±1.67) [60.00,64.18]	65.58 (±1.21) [64.11,67.08]
$D_{3,2}$ (μm)	68.95 (±1.28) [67.50,70.54]	60.43 (±4.14) [53.14,63.41]	50.80 (±1.57) [49.48,53.14]	55.00 (±2.37) [50.96,56.77]	59.33 (±1.63) [57.24,61.68]	62.72 (±1.45) [60.69,64.54]
$D_{4,3}$ (μm)	75.78 (±1.63) [73.86,77.90]	67.05 (±3.74) [60.56,69.00]	57.49 (±1.96) [55.88,60.56]	61.47 (±2.78) [56.53,63.22]	65.92 (±2.35) [63.63,69.87]	69.63 (±1.77) [67.27,71.98]
δ	4.25 (±0.39) [3.78,4.74]	3.41 (±0.21) [3.18,3.65]	3.59 (±0.18) [3.34,3.78]	3.75 (±0.34) [3.27,4.10]	3.91 (±0.19) [3.71,4.21]	4.05 (±0.22) [3.75,4.28]

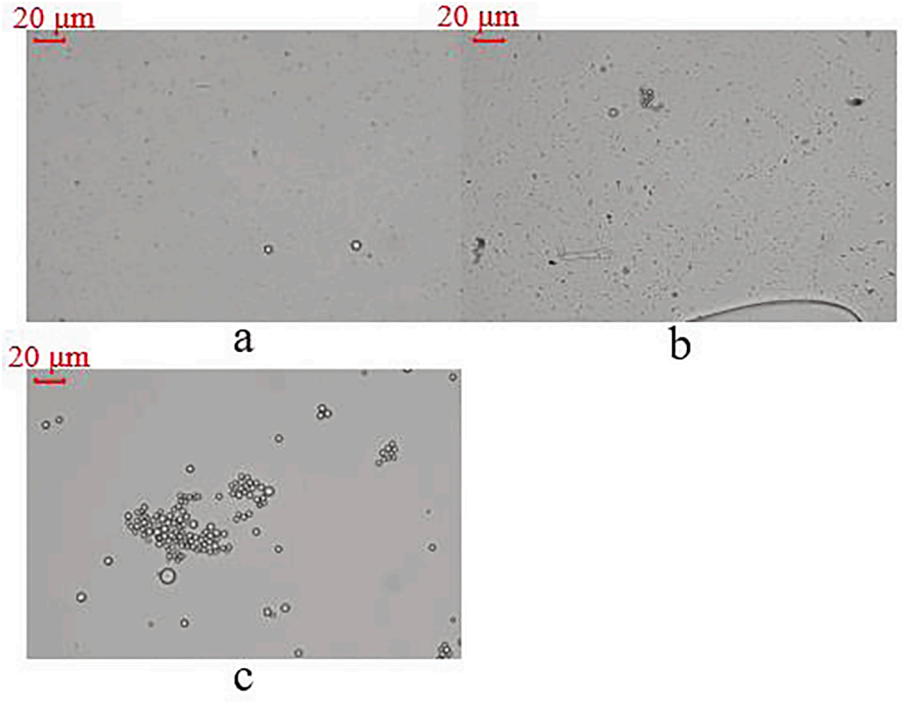

Fig. 6. Microscopic images of emulsion droplets prepared by ultrasound underdifferent conditions of (a) 20% – 6 min, (b) 50% – 6 min, and (c) 50% – 10 min.

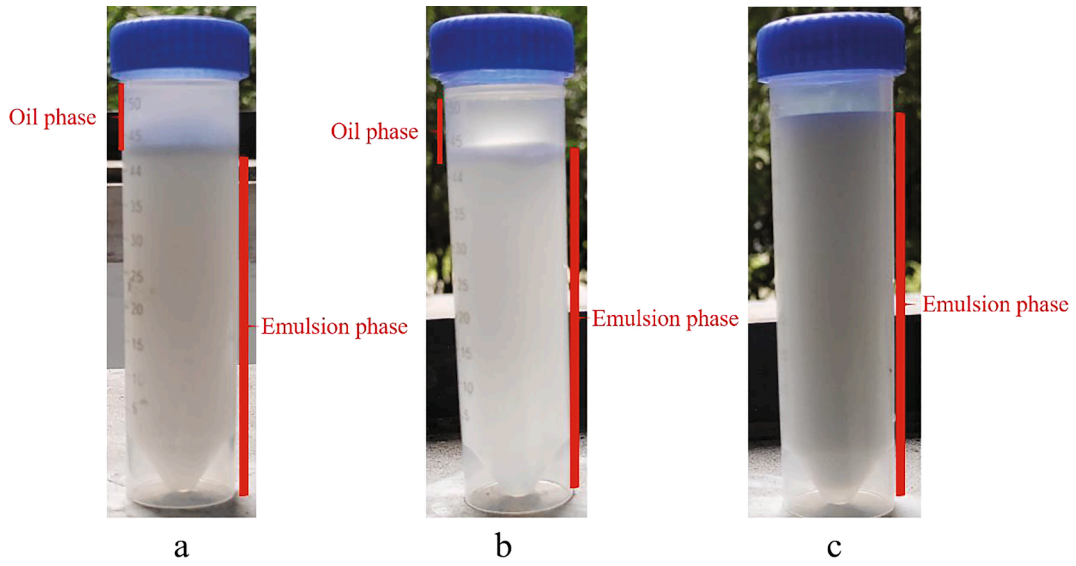

Fig. 7. Macro photo of emulsion prepared by ultrasound at different conditions (a) 50% – 10 min, (b) 50% – 20 min, and (c) 80% – 10 min.

the conductivity of the samples. The binding energy was corrected based on the C–C bond of 284.8 eV in the C element.

3. Results and discussions

3.1. R-SH

3.1.1. Intensity

For the sake of description, emulsions with a chord length of a to b μm should be defined as an emulsion (a - b). The emulsions are prepared by R-SH under different intensities, with 6 min emulsification time. The optical microscopic images and the chord length of the emulsions are shown in Fig. 2 and Fig. 3, respectively. The chord lengths d_{10}, d_{50}, d_{90}, $D_{3,2}$, $D_{4,3}$, and δ of the emulsions are presented in Table 3. Fig. 2, and Fig. 3 show the measurement results of emulsion droplet sizes provided by the optical microscope and FBRM, respectively.

The presented results in Fig. 2 indicate a significant difference in the number of coarse droplets nucleated within the emulsion under the examined four intensities. Fig. 3a displays two peaks in the distribution of emulsion droplets, consistent with the δ given in Table 3. As shown in Fig. 3b, the composition of the emulsion (<10) is less at 10,000 rpm, and significant differences exist in emulsion (>30).Table 3 indicates that with the increase in R-SH intensity, the d_{50} of emulsion keeps getting smaller, and the d_{90} of emulsion initially decreases and then increases. In this context, Jafari et al. pointed out that the emulsion droplet size could not be reduced with energy input below a certain size [39]. Thus, continuing to input energy might be inefficient or sometimes could increase the emulsion droplet size because of poor stabilization of the newly formed droplets. Therefore, as R-SH time or R-SH intensity increase, there is an inflection point in the size of the emulsion droplets, and the size of emulsion droplets begin to increase after the inflection point. Thus, 16,000 rpm with the lowest $D_{3,2}$, $D_{4,3}$, and δ is chosen for further assessments.

3.1.2. Time

R-SH prepared the emulsions at different times, and the R-SH intensity was 16,000 rpm. The optical microscopic images and the chord length of the emulsions are shown in Fig. 4 and Fig. 5, respectively. The chord lengths d_{10}, d_{50}, d_{90}, $D_{3,2}$, $D_{4,3}$, and δ of the emulsions are presented in Table 4 in detail.

Fig. 5 and Table 4 show the law of emulsion droplet size change in terms of R-SH time. As time increases, the emulsion's droplet size first decreases and then increases, consistent with the research conclusion [40]. It can be seen from Fig. 4 that unlike the effect of R-SH strength on the emulsion, the effect of R-SH time on the emulsion is quite significant, also complemented by Fig. 5. The larger range of time variables causes this phenomenon, and the law of the three curves of 6, 8, and 12 min is similar to the law of R-SH intensity change. Therefore, relative to the intensity determined by the equipment, it is necessary to explore a good R-SH time. There are still two peaks in the curve in Fig. 5 (a). 4 min with the minimum d_{50}, $D_{3,2}$, and $D_{4,3}$ is the most suitable condition.

3.2. Ultrasound

The composition of the water phase observed through the microscope is shown in Fig. 6. It illustrates that ultrasound emulsifies the oil phase to form smaller oil droplets than R-SH but with substantially lower efficiency. However, outcomes of the ultrasound process for Pickering emulsion preparation indicated that this procedure could not prepare a stable emulsion (Fig. 7a). This phenomenon could be due to the dispersion area of R-SH having a larger volume, which results in a lower average power density [41]. Unlike R-SH, the ultrasound energy is concentrated near the probe, causing cavitation. It can prepare an emulsion with smaller emulsion droplets, but the efficiency is also lower [42]. The test results given in Fig. 6 are consistent with the above literature. Compared with R-SH, ultrasound is difficult to form a stable emulsion under the condition of low power or short time, which shows the lower efficiency of ultrasound. As shown in Fig. 6, under the conditions of 20% – 6 min, 50% – 6 min, 50% – 10 min, the emulsion is difficult to stabilize, and the emulsion droplets are difficult to form. As shown in Fig. 6 (a), few droplets are observed under the condition of 20% – 6 min. When the ultrasonic intensity is increased from 20% to 50%, as shown in Fig. 6 (b), the agglomeration of droplets is observed. In addition to that, the agglomeration of droplets is obvious when ultrasonic time is increased from 6 min to 10 min, as shown in Fig. 6 (c).

As the input energy increases, the number of emulsion droplets in the emulsified phase grows. It can be inferred that if just ultrasound is used, a significant ultrasound intensity or ultrasound time would probably be required to obtain a uniform emulsion. However, results indicated that a uniform emulsion could not be obtained when the ultrasound time increases (Fig. 7 b), while increasing the ultrasound intensity led to the formation of uniform emulsion (Fig. 7 c). In addition, the size of the emulsion droplets formed by ultrasound is smaller with a more uniform particle size compared to the R-SH results; however, the efficiency of forming emulsion is lower. Cavitation in the ultrasonic treatment could violently form vapor cavities in the liquid, generating local high

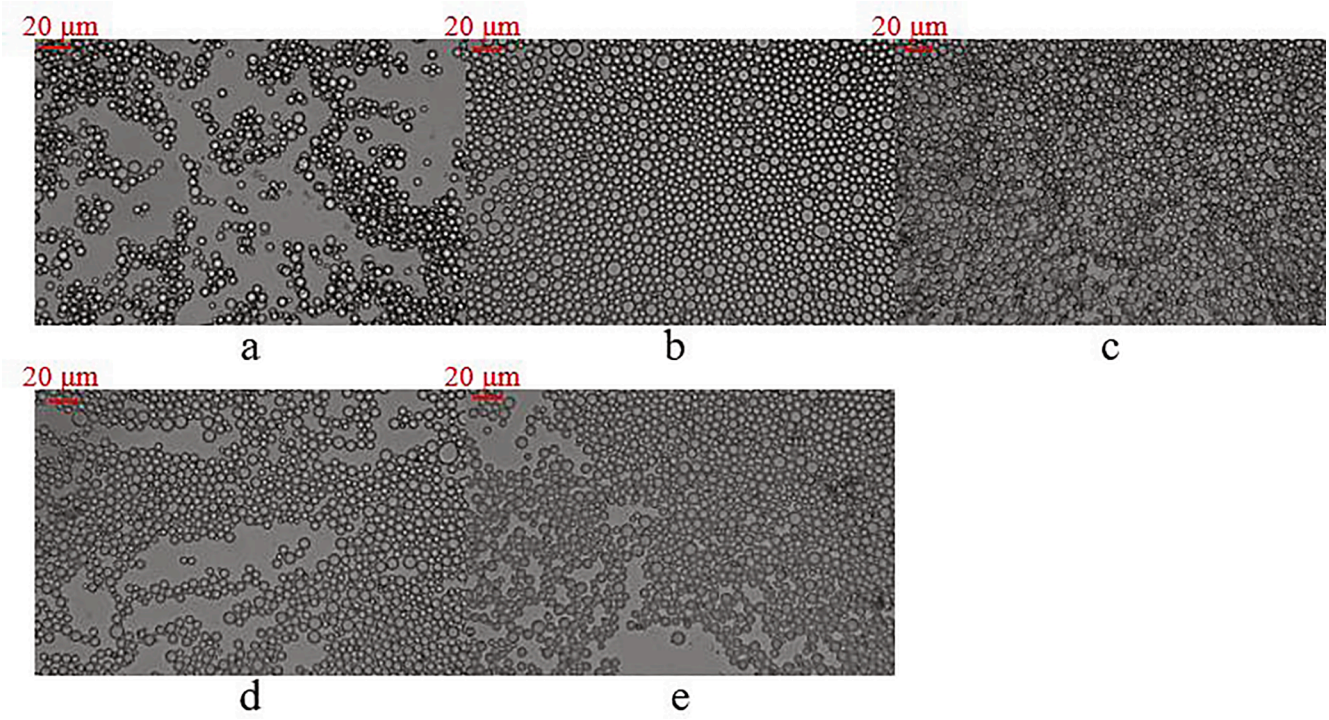

Fig. 8. Optical microscopic images of emulsion droplets prepared by the combined process of R-SH (16,000 rpm − 4 min) and ultrasound at different times (a) 1, (b) 2, (c) 4, (d) 6, and (e) 8 min.

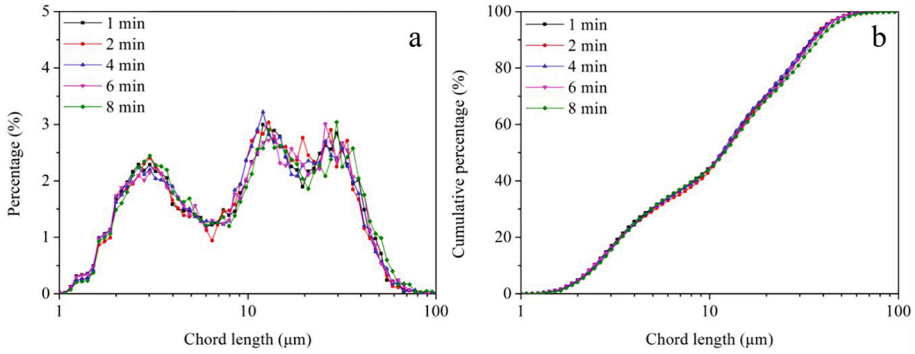

Fig. 9. Chord length of emulsion droplets prepared by the combined process of R-SH and ultrasound at different times (a is distribution curve, and b is accumulation curve).

Table 5
d_{10}, d_{50}, d_{90}, $D_{3,2}$, $D_{4,3}$ and δ of emulsion droplets prepared by the combined process of R-SH and ultrasound at different times.

Average diameter	Ultrasound time (min)				
	1	2	4	6	8
d_{10} (μm)	2.43 (±0.08) [2.33,2.50]	2.55 (±0.12) [2.37,2.71]	2.48 (±0.11) [2.31,2.56]	2.41 (±0.05) [2.35,2.49]	2.51 (±0.08) [2.39,2.57]
d_{50} (μm)	11.76 (±0.56) [11.25,12.63]	11.86 (±0.12) [11.78,12.06]	11.60 (±0.19) [11.40,11.91]	11.74 (±0.45) [10.94,11.98]	11.87 (±0.70) [11.06,12.80]
d_{90} (μm)	35.34 (±0.84) [34.16,36.14]	34.33 (±0.48) [33.60,34.78]	34.40 (±1.28) [33.12,36.38]	35.63 (±0.52) [34.96,36.30]	37.44 (±0.83) [36.50,38.71]
$D_{3,2}$ (μm)	34.84 (±1.01) [33.77,35.80]	34.95 (±0.90) [34.07,36.31]	35.28 (±1.47) [33.68,37.27]	35.84 (±1.43) [34.17,38.11]	39.01 (±1.34) [37.62,40.42]
$D_{4,3}$ (μm)	40.71 (±1.54) [38.99,42.13]	42.50 (±2.46) [40.19,46.03]	42.32 (±2.33) [39.07,44.28]	42.43 (±2.75) [39.41,46.62]	47.10 (±2.72) [43.36,49.64]
δ	2.80 (±0.15) [2.63,3.01]	2.68 (±0.06) [2.62,2.74]	2.75 (±0.12) [2.64,2.95]	2.83 (±0.09) [2.76,2.98]	2.95 (±0.12) [2.83,3.12]

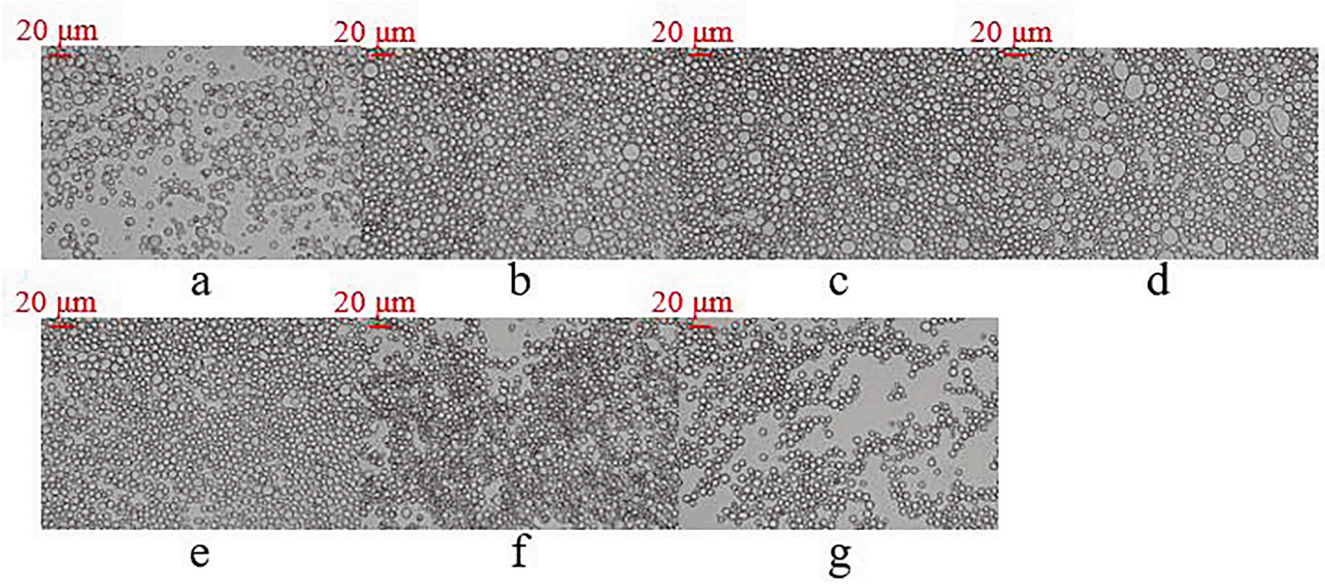

Fig. 10. Optical microscope images of emulsion droplets prepared by the combined process of R-SH (16,000 rpm – 4 min) and ultrasound with different intensities: (a) 20, (b) 30, (c) 40, (d) 50, (e) 60, (f) 80, and (g) 100%.

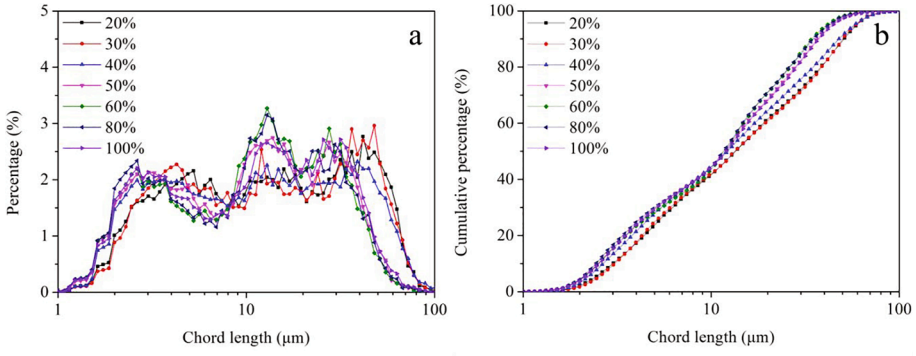

Fig. 11. Chord length of emulsion droplets prepared by the combined process of R-SH and ultrasound with different intensities (a is distribution curve, and b is accumulation curve).

pressure, stress, and temperature, leading to the formation of emulsions. But since breaking an interface requires a large amount of energy, it is better to first prepare an emulsion before applying ultrasound treatment [40].

The influence of ultrasound time and intensity was studied in detail for a combined process "R-SH and ultrasound" to explore the effect of ultrasound on emulsion stability.

3.3. Combined process (R-SH and ultrasound)

3.3.1. Ultrasound time

Section 3.2 shows that ultrasonic intensity greatly influences the emulsion, especially at high intensity. Therefore, the emulsion is first treated with R-SH at 16000 rpm for 4 min and then further emulsified by ultrasound at different times with 80% ultrasound intensity. The optical

Table 6
d_{10}, d_{50}, d_{90}, $D_{3,2}$, $D_{4,3}$, and δ of emulsion droplets prepared by the combined process of R-SH and ultrasound with different intensities.

Average diameter	Ultrasound intensity (%)						
	20	30	40	50	60	80	100
d_{10} (μm)	3.01 (±0.09) [2.87,3.08]	3.30 (±0.39) [3.06,3.99]	2.63 (±0.11) [2.53,2.79]	2.53 (±0.06) [2.48,2.62]	2.50 (±0.08) [2.37,2.57]	2.44 (±0.10) [2.28,2.51]	2.52 (±0.05) [2.44,2.56]
d_{50} (μm)	13.59 (±0.59) [12.89,14.42]	13.49 (±1.09) [12.58,15.31]	11.89 (±0.72) [11.21,12.96]	11.45 (±0.38) [10.80,11.75]	11.87 (±0.30) [11.62,12.38]	11.61 (±0.52) [10.82,12.22]	11.91 (±0.41) [11.42,12.34]
d_{90} (μm)	50.50 (±0.82) [49.12,51.27]	49.91 (±1.37) [47.78,51.51]	47.80 (±1.78) [45.07,50.01]	36.00 (±1.10) [34.78,36.95]	34.35 (±1.01) [33.18,35.59]	34.82 (±1.26) [33.91,36.18]	36.96 (±0.66) [36.31,38.00]
$D_{3,2}$ (μm)	49.44 (±0.70) [48.72,50.44]	49.38 (±1.05) [48.04,50.34]	49.56 (±1.43) [47.68,50.84]	36.73 (±1.16) [34.71,37.49]	35.48 (±1.13) [34.24,37.28]	37.01 (±1.80) [34.40,39.28]	38.39 (±2.02) [35.58,41.26]
$D_{4,3}$ (μm)	56.56 (±1.19) [55.39,57.87]	56.58 (±1.61) [54.60,58.41]	57.99 (±1.86) [55.86,60.22]	43.66 (±2.25) [40.38,46.50]	43.31 (±2.33) [41.38,46.79]	45.30 (±4.24) [40.47,52.07]	46.04 (±3.55) [41.09,50.94]
δ	3.50 (±0.12) [3.30,3.59]	3.47 (±0.22) [3.15,3.72]	3.80 (±0.16) [3.64,4.00]	2.92 (±0.09) [2.78,2.99]	2.69 (±0.10) [2.60,2.85]	2.79 (±0.11) [2.69,2.97]	2.89 (±0.13) [2.78,3.08]

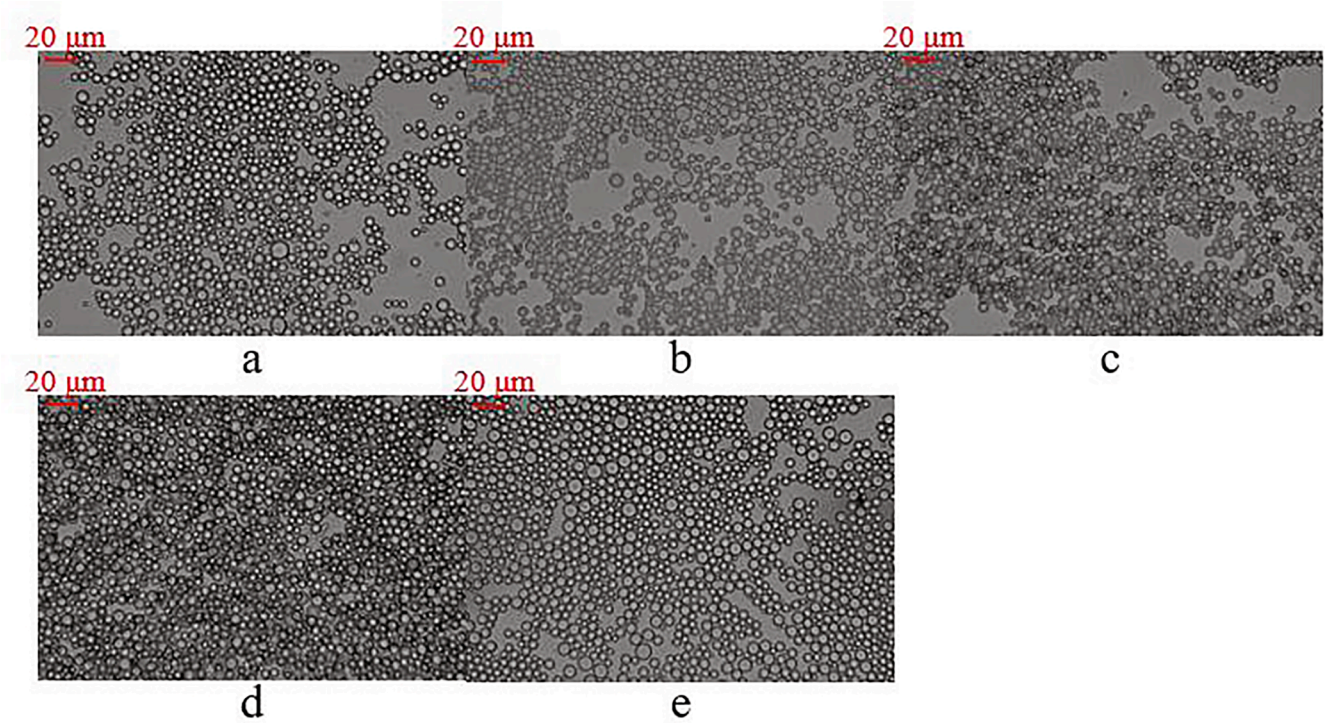

Fig. 12. Optical microscope images of emulsion droplets prepared by the combined process of R-SH with different times (a is for 1 min, b is for 2 min, c is for 4 min, d is for 6 min, e is for 8 min) and ultrasound (60% – 4 min).

microscope images and the chord length of the emulsions are shown in Fig. 8 and Fig. 9, respectively. The chord length indicators, including d_{10}, d_{50}, d_{90}, $D_{3,2}$, $D_{4,3}$, and δ of the emulsions, are shown in Table 5.

A comparison between, Fig. 2, Fig. 4, and Fig. 8 shows that large droplets are significantly reduced, and they became more uniform as a result of combining methods. Chord length results also complemented these outcomes. Compared with R-SH, the peaks of the emulsion distribution curve in Fig. 9 (a) became three, wherein the content of emulsion (20–100) was significantly reduced, and emulsion (10–20) was significantly increased. As shown in Fig. 9, it is clear that the effect of ultrasound time on the emulsion is not significant on the emulsion, which is also reflected in Table 5. It can be seen from Table 5 that 4 min treatment with the smallest d_{50} and $D_{4,3}$ is the follow-up research condition.

3.3.2. *Ultrasound intensity*

The emulsion is first treated with R-SH at 16,000 rpm for 4 min and then further emulsified under different intensities by ultrasound for 4 min. The optical microscopic images and the chord length of the emulsions are shown in Fig. 10 and Fig. 11. The chord lengths d_{10}, d_{50}, d_{90}, $D_{3,2}$, $D_{4,3}$, and δ of the emulsions are shown in Table 6.

Fig. 10 shows that the content of coarse emulsion decreased significantly with the increase of ultrasonic intensity. The curves in Fig. 11 show that, unlike ultrasound time, the ultrasonic intensity has more influence on the emulsion droplets' size. The ultrasonic intensity has a greater influence on the emulsion particle size (as marked in Section 3.2). Gaikwad et al. [43] observed that as the dispersed phase hold-up increases with an increase in the ultrasound time, the collision frequency of droplets increases, resulting in the coalescence of small droplets to form large droplets, which are relatively stable at lower ultrasound intensity levels. However, such coalescence is not observed at high ultrasound intensity, and the droplet size shows a continuous decrease or an asymptotic behavior concerning time. As the ultrasound intensity increases, the pressure amplitude of the applied ultrasound increases, causing an increase in the cavitation phenomena, and as the cavitation increases, the large droplets frequently break to form smaller droplets. Hence, there is a decrease in the emulsion droplet size with an increase in the ultrasound intensity. But convergent agglomeration may

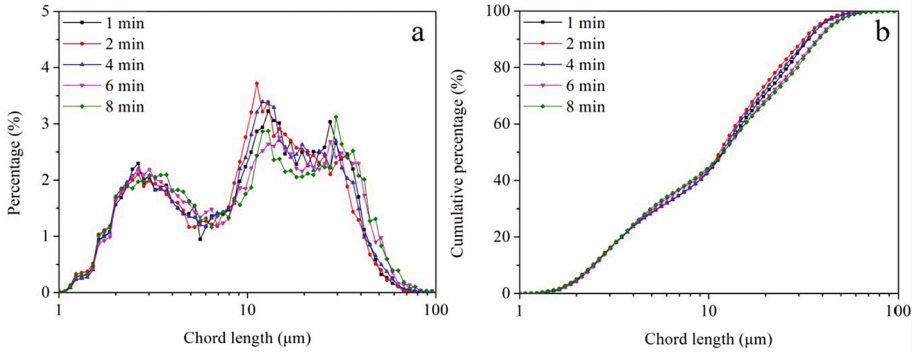

Fig. 13. Chord length of emulsion droplets prepared by the combined process of R-SH with different times and ultrasound (60% – 4 min) (a is distribution curve, and b is accumulation curve).

Table 7
d_{10}, d_{50}, d_{90}, $D_{3,2}$, $D_{4,3}$ and δ of emulsion droplets prepared by the combined process of R-SH with different times and ultrasound (60% − 4 min).

Average diameter	R-SH time (min)				
	1	2	4	6	8
d_{10} (μm)	2.50 (±0.05) [2.43,2.56]	2.41 (±0.08) [2.32,2.53]	2.48 (±0.05) [2.40,2.53]	2.47 (±0.05) [2.41,2.55]	2.44 (±0.08) [2.36,2.52]
d_{50} (μm)	11.89 (±0.41) [11.48,12.53]	11.40 (±0.29) [10.99,11.77]	11.81 (±0.41) [11.31,12.31]	11.85 (±0.45) [11.45,12.49]	12.09 (±0.54) [11.52,12.87]
d_{90} (μm)	33.87 (±1.42) [31.61,35.16]	31.96 (±0.64) [31.28,32.76]	33.18 (±0.79) [32.15,34.25]	37.29 (±1.80) [35.49,39.50]	38.25 (±0.73) [37.11,39.05]
$D_{3,2}$ (μm)	33.90 (±0.78) [32.88,34.78]	32.58 (±0.75) [31.60,33.57]	34.21 (±1.04) [32.61,35.37]	38.08 (±1.11) [37.18,39.78]	39.21, (±1.29) [38.02,41.10]
$D_{4,3}$ (μm)	40.89 (±1.16) [39.23,42.20]	39.56 (±1.62) [37.56,41.73]	41.64 (±2.33) [39.12,45.48]	45.42 (±0.97) [43.84,46.20]	46.19 (±2.24) [43.51,49.43]
δ	2.64 (±0.09) [2.54,2.76]	2.59 (±0.05) [2.52,2.65]	2.60 (±0.08) [2.47,2.68]	2.92 (±0.10) [2.78,3.06]	2.97 (±0.17) [2.70,3.14]

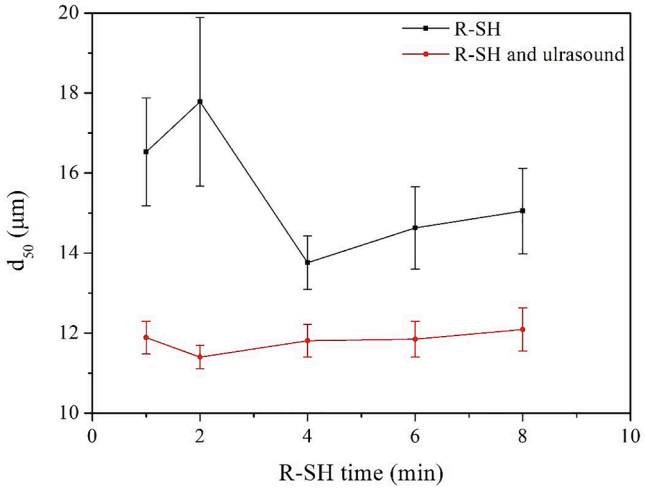

Fig. 14. Comparison of d_{50} of emulsion prepared by R-SH process (16,000 rpm) and R-SH ultrasonic combined process over R-SH time (the ultrasonic intensity was 60%, the ultrasonic time was 4 min).

dominate when the optimal ultrasound intensity is exceeded [44]. This is why when the ultrasonic intensity reaches 100%, the emulsion droplets enlarge, as shown in Fig. 11. When the ultrasonic intensity reaches 80%, the emulsion droplets approach the smallest d_{50} but don't achieve the smallest $D_{4,3}$. Therefore, 60% of ultrasound intensity with the smallest $D_{4,3}$ is chosen for further assessments.

3.3.3. R-SH time

For exploring the influence of R-SH time on the emulsion droplets prepared by the combined process (R-SH and ultrasound), the emulsion is first treated with R-SH at 16000 rpm for different times and then

Table 8
d_{10}, d_{50}, d_{90}, $D_{3,2}$, $D_{4,3}$ and δ of emulsion droplets prepared by the combined process of R-SH and ultrasonic method.

Average diameter	The combined "R-SH + Ultrasound" time (min)			
	2 min + 0 min	2 min + 4 min	4 min + 2 min	6 min + 0 min
d_{10} (μm)	4.28 (±0.56) [3.34,4.69]	2.41 (±0.08) [2.32,2.53]	2.55 (±0.12) [2.37,2.71]	3.48 (±0.09) [3.35,3.56]
d_{50} (μm)	17.78 (±2.11) [14.32,19.49]	11.40 (±0.29) [10.99,11.77]	11.86 (±0.12) [11.78,12.06]	14.63 (±1.03) [13.71,15.82]
d_{90} (μm)	64.61 (±5.82) [54.25,67.13]	31.96 (±0.64) [31.28,32.76]	34.33 (±0.48) [33.60,34.78]	58.09 (±2.41) [54.73,60.24]
$D_{3,2}$ (μm)	60.43 (±4.14) [53.14,63.41]	32.58 (±0.75) [31.60,33.57]	34.95 (±0.90) [34.07,36.31]	55.00 (±2.37) [50.96,56.77]
$D_{4,3}$ (μm)	67.05 (±3.74) [60.56,69.00]	39.56 (±1.62) [37.56,41.73]	42.50 (±2.46) [40.19,46.03]	61.47 (±2.78) [56.53,63.22]
δ	3.41 (±0.21) [3.18,3.65]	2.59 (±0.05) [2.52,2.65]	2.68 (±0.06) [2.62,2.74]	3.75 (±0.34) [3.27,4.10]

further emulsified for 4 min by ultrasound with 60% intensity. The optical microscope images and the chord length of the emulsions are shown in Fig. 12 and Fig. 13. The chord lengths d_{10}, d_{50}, d_{90}, $D_{3,2}$, $D_{4,3}$, and δ of the emulsions are shown in Table 7. Results (Fig. 12) show that the particle size of the emulsion is relatively uniform. However, as shown in Fig. 13, there is a big difference in the size of droplets in emulsion (>10). This means that ultrasound has a significant effect on the emulsion (<10) and the effect of R-SH on the emulsion is not visible. The data in Table 7 indicates that when the R-SH time is 2 min, the d_{50}, $D_{3,2}$, and $D_{4,3}$ of emulsion are the smallest, rather than at 4 min (Table 4).

Fig. 14 compares the d_{50} of emulsion prepared by the R-SH process and R-SH ultrasonic combined process over R-SH time for further assessments. These outcomes illustrate that at 4 min, d_{50} of the emulsion after R-SH treatment has the shortest distance from the d_{50} of the emulsion after the optimum ultrasonic conditions, indicating d_{50} of the

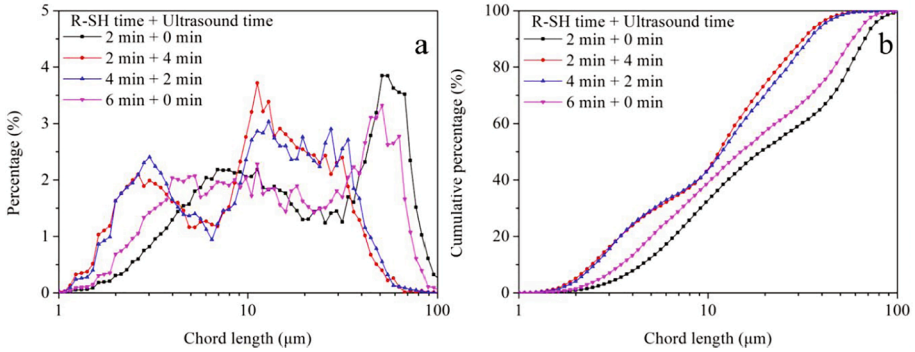

Fig. 15. The comparison of R-SH and the combined process (R-SH and ultrasonic) (a is distribution curve, and b is accumulation curve).

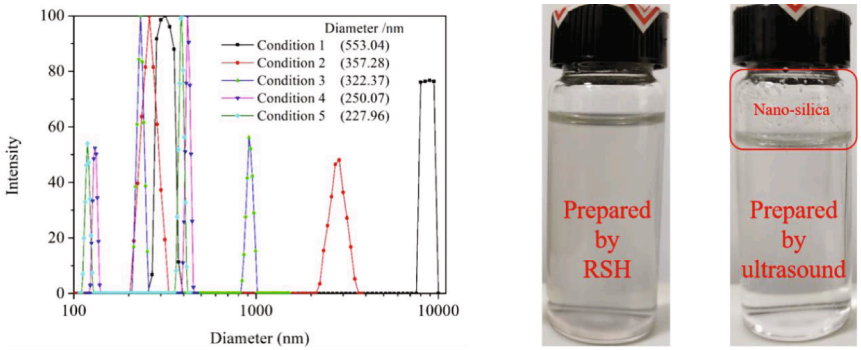

Condition 1	R-SH prepared at 10000 rpm for 4 min
Condition 2	R-SH prepared at 16000 rpm for 4 min
Condition 3	R-SH prepared at 16000 rpm for 8 min
Condition 4	R-SH prepared at 16000 rpm for 4 min and ultrasound prepared at 20% for 4 min
Condition 5	R-SH prepared at 16000 rpm for 4 min and ultrasound prepared at 60% for 4 min

Fig. 16. (a) Particle size distribution of nano-silica under different conditions; (b) uniform nano-silica/water solution after treatment by R-SH, and (c) nano-silica and water after treatment by ultrasonic.

emulsion droplets experienced the minor variation (having the little benefit of sonication). This phenomenon could be because ultrasound significantly reduces emulsion droplets than R-SH. Though, as the emulsion droplets are reduced to a certain extent, the effect of ultrasound will be counterproductive, as presented in Table 5. Therefore, it is pertinent to appropriately reduce the R-SH processing time, reduce the emulsion droplets by ultrasound, obtain smaller emulsions and save energy.

3.4. R-SH vs. The combined process

Fig. 15 comprehensively compares R-SH with the combined process (R-SH and ultrasound). The corresponding curves for d_{10}, d_{50}, d_{90}, $D_{3,2}$, $D_{4,3}$, and δ are shown in Table 8.

From the comparison of the three curves for different R-SH and ultrasonic treatment times, i.e. "2 min + 0 min", "2 min + 4 min" and "6 min + 0 min" (Fig. 15), it can be seen that for 4 min of R-SH or 4 min of ultrasound applied after 2 min of R-SH, the effect of ultrasonic treatment is relatively higher than R-SH. This also shows that ultrasound is superior to R-SH in reducing the size of the emulsion droplets. The d_{50}, $D_{3,2}$, $D_{4,3}$ listed in Table 8 also support this statement. When the treatment time is the same, the three curves of "2 min + 4 min", "4 min + 2 min" and "6 min + 0 min" in Fig. 15 show that the short-time ultrasonic treatment can also reduce the emulsion droplet size. The curves of "2 min + 4 min" and "4 min + 2 min" illustrate a big difference in the part where the chord length is>15 μm, indicating that ultrasound significantly reduces emulsion (>15). This is consistent with the results presented in Table 8.

And from Table 8, the δ of the emulsion was significantly reduced after ultrasonic treatment. The emulsion was treated by ultrasound to become more monodisperse, as shown in Fig. 15 (a). The emulsion (>40) for "2 min + 0 min" vs. "6 min + 0 min" represent the main particle size distribution for only R-SH. With the increase of R-SH time, the number of emulsions (<10) increases significantly (i.e., the number of emulsions (>30) decreased significantly). The comparison of the two curves, "2 min + 0 min" vs. "2 min + 4 min" shows that ultrasound can effectively disperse emulsion (>40) and significantly increases the content of emulsion (<10). The comparison of the two curves, "2 min + 4 min" vs. "4 min + 2 min" indicates that the increase of the ultrasonic time can further disperse the emulsion (>30). The particle size distribution of nano-silica under different conditions has been measured as illustrated in Fig. 16. From the conditions 1, 2, and 3 in Fig. 16 (a), it is evident that as R-SH intensity and time increase, the two peaks of NSP distribution indicate the particle size decrease. Large emulsion droplets are formed due to the aggregated NSP. R-SH dispersed nano-silica still has micron-sized aggregate particles, which occupy the nanoparticles as emulsifiers and contribute to the formation of large emulsion droplets. This is also why the emulsion distribution presents two peaks, and the peak value of emulsion (>30) is high.

Table 9
A comparison within different process setups in their optimum points.

Condition	Optimum R-SH	R-SH + optimum ultrasound	Optimum (R-SH + ultrasound)
d_{10}	3.20 (±0.15) [3.05,3.35]	2.50 (±0.08) [2.37,2.57]	2.41 (±0.08) [2.32,2.53]
d_{50}	13.76 (±0.67) [13.00,14.53]	11.87 (±0.30) [11.62,12.38]	11.40 (±0.29) [10.99,11.77]
d_{90}	52.46 (±1.15) [51.62,54.28]	34.35 (±1.01) [33.18,35.59]	31.96 (±0.64) [31.28,32.76]
$D_{3,2}$	50.80 (±1.57) [49.48,53.14]	35.48 (±1.13) [34.24,37.28]	32.58 (±0.75) [31.60,33.57]
$D_{4,3}$	57.49 (±1.96) [55.88,60.56]	43.31 (±2.33) [41.38,46.79]	39.56 (±1.62) [37.56,41.73]
δ	3.59 (±0.18) [3.34,3.78]	2.69 (±0.10) [2.60,2.85]	2.59 (±0.05) [2.52,2.65]

The nano-silica after ultrasonic treatment is shown in Fig. 16 (c). NSP cannot be completely dispersed in water, as most of them float on the surface of the water. Compared with the nano-silica prepared by ultrasound, the nano-silica prepared by R-SH is a uniform solution, as demonstrated in Fig. 16 (b). It can be seen that R-SH is inferior to ultrasound in nano-level dispersion, but it is better than ultrasound in macroscopic dispersion. The dispersing effect of ultrasound is discussed under the combined process conditions. It can be seen from conditions 2, 4, and 5 in Fig. 16 (a) that ultrasound is beneficial to the dispersion of micron-sized aggregates, where the emulsion droplets after ultrasound treatment become smaller. As the ultrasonic intensity increases, the NSP becomes more dispersed. The dispersion effect of nano-silica prepared by R-SH or ultrasound is evidently related to the droplet size of the emulsion. It is worth noting that although the NSP are further dispersed,

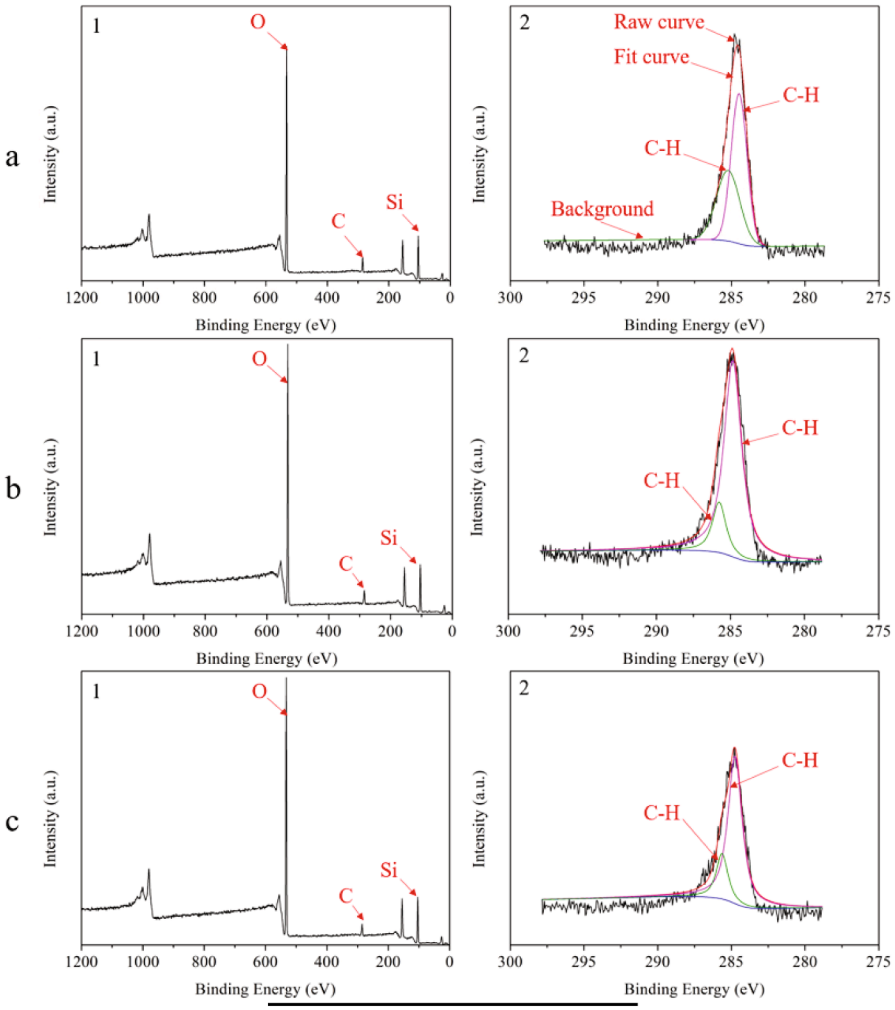

Name	O	C	Si
a-atomic %	62.09	10.03	27.87
b-atomic %	63.45	9.36	27.19
c-atomic %	63.19	9.34	27.47

Fig. 17. The XPS results of the nano-silica particles (a is for the nano-silica particles, b is for the nano-silica particles after R-SH, c is for the nano-silica particles after ultrasonic).

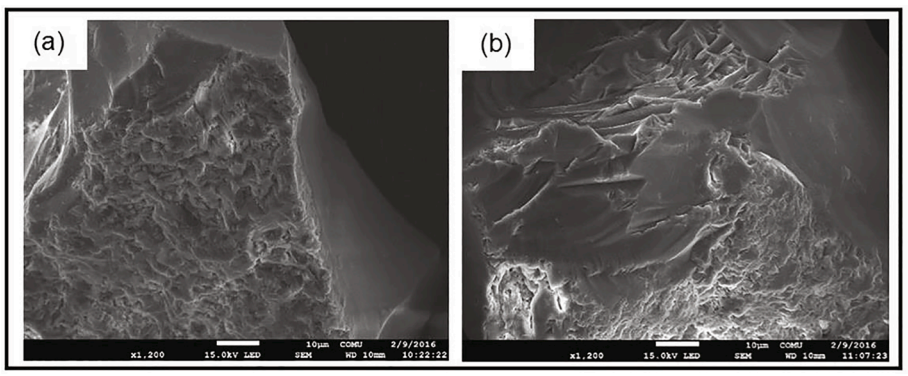

Fig. 18. SEM images of 75–150 μm quartz samples (a) without and (b) with ultrasound (30 W) at × 1200 magnification rate [46].

they still exist as aggregates. Table 9 summarizes the results of various methods in their optimum points.

In addition to the dispersion of nanoparticles, their surface properties also influence the preparation of Pickering emulsion [45]. Thus, the hydrophobicity, zeta potential, and morphological characteristics of NSP with and without mechanical treatment were discussed. First, Fig. 17 indicates that the R-SH and ultrasonic treatment processes have almost no influence on the surface of NSP. The contents ratio of O, C, and

Table 10
The zeta potential of the nano-silica particles under different treatment conditions.

Sample	Zeta potential (mV)
The nano-silica particles	−37.29 (±1.75)
The nano-silica particles after R-SH	−37.87 (±1.84)
The nano-silica particles after ultrasonic	−38.92 (±1.96

Si are quite close in samples under different conditions, which indicates that the treatment of NSP by the mechanical processes cannot change the hydrophobicity of NSP. In this regard, Gungoren [46] compared the SEM images of −75 + 150 μm quartz particles with and without ultrasound (Fig. 18). It is indicated that there was no significant change on the particle surface for the ultrasonic treatment. Due to the resolution limitation of the SEM device, it is difficult to obtain clear images to observe the morphological characteristics of NSP. Quartz is a homogeneous mineral, and its properties are the same for different diameters of particles. Thus, it is considered that the mechanical processes cannot change the morphological features of NSP. Finally, Table 10 summarizes the zeta potential data of the NSP. Samples under different conditions have almost the same zeta potential levels. Following this, Blake and Ralston reported that the NSP zeta potential remained unchanged after hydrophobization by trimethylchlorosilane [47]. Overall, it is concluded that the effects of R-SH and ultrasonic treatment processes on the surface properties of NSP are insignificant.

4. Conclusions

Exploring the effectiveness of various mechanical processes (R-SH, ultrasonic emulsification, and their combination) for Pickering emulsion preparation by using nano-silica particles indicated that:

- Outcomes demonstrated that due to equipment limitation, the intensity adjustment of R-SH is not as wide as the time adjustment range, making R-SH more strongly affected by time.
- The nano-silica particles after ultrasonic treatment were more dispersed, and the emulsion droplets were smaller and more monodispersed.
- Ultrasonic intensity is far more important than ultrasonic time, which is related to the formation of the smaller emulsion. Ultrasound treatment could obtain smaller emulsion droplets than R-SH, but it requires great ultrasound intensity to prepare a uniform emulsion.
- Comparing the ultrasound vs. R-SH, the longer time and greater strength required to obtain stable emulsions and R-SH could not effectively disperse NSP. Results illustrated that R-SH and optimal ultrasound as a combined process is more effective than the ultrasound lonely.
- The optimum combination (R-SH with 16000 rpm for 2 min and ultrasound with 60% for 4 min) showed an optimal condition that facilitates the use of less energy to obtain the smallest droplets.

CRediT authorship contribution statement

Jixuan Gao: Conceptualization, Investigation, Software, Writing – original draft. **Xiangning Bu:** Conceptualization, Writing – review & editing, Funding acquisition, Methodology. **Shaoqi Zhou:** Conceptualization. **Xuexia Wang:** Conceptualization, Investigation, Software, Writing – original draft. **Muhammad Bilal:** Writing – review & editing, Formal analysis. **Fawad Ul Hassan:** Writing – review & editing, Formal analysis. **Ahmad Hassanzadeh:** Writing – review & editing, Formal analysis. **Guangyuan Xie:** Supervision. **Saeed Chehreh Chelgani:** Writing – review & editing, Formal analysis.

Declaration of Competing Interest

The authors declare that they have no known competing financial interests or personal relationships that could have appeared to influence the work reported in this paper.

Acknowledgments

The authors gratefully acknowledge financial support from the Project funded by the China Postdoctoral Science Foundation (No. 2019M652024) and the National Nature Science Foundation of China (Grant No. 52074288).

Appendix A. Supplementary data

Supplementary data to this article can be found online at https://doi.org/10.1016/j.ultsonch.2022.105928.

References

[1] Y. Chevalier, M.A. Bolzinger, Emulsions stabilized with solid nanoparticles: Pickering emulsions, Colloids Surf., A 439 (2013) 23–34.
[2] R. Aveyard, B.P. Binks, J.H. Clint, Emulsions stabilised solely by colloidal particles, Adv. Colloid Interface Sci. 100-102 (2003) 503–546.
[3] B.P. Binks, Particles as surfactants—similarities and differences, Curr. Opin Colloid Interface Sci. 7 (1-2) (2002) 21–41.
[4] L. Chen, F. Ao, X. Ge, W. Shen, Food-grade pickering emulsions: preparation, stabilization and applications, Molecules 25 (14) (2020).
[5] S. Abend, G. Lagaly, Bentonite and double hydroxides as emulsifying agents, Clay Miner. 36 (4) (2001) 557–570.
[6] A. Gelot, W. Friesen, H.A. Hamza, Emulsification of oil and water in the presence of finely divided solids and surface-active agents, Colloids Surf. 12 (none) (1984) 271–303.
[7] A.L.R. Costa, A. Gomes, G.D.F. Furtado, H. Tibolla, R.L. Cunha, Modulating in vitro digestibility of Pickering emulsions stabilized by food-grade polysaccharides particles, Carbohydr. Polym. 227 (2019), 115344.
[8] F. Gautier, M. Destribats, R. Perrier-Cornet, J.-F.O. Dechézelles, J. Giermanska, V. Héroguez, S. Ravaine, F. Leal-Calderon, V. Schmitt, Pickering emulsions with stimulable particles: from highly- to weakly-covered interfaces, Phys. Chem. Chem. Phys. 9 (48) (2007) 6455–6462.
[9] B.P. Binks, S.O. Lumsdon, Stability of oil-in-water emulsions stabilised by silica particles, PCCP 1 (12) (1999) 3007–3016.
[10] B.P. Binks, S.O. Lumsdon, Influence of particle wettability on the type and stability of surfactant-free emulsions, Langmuir 16 (23) (2000) 8622–8631.
[11] B.P. Binks, J.H. Clint, Solid wettability from surface energy components: relevance to pickering emulsions, Langmuir 18 (4) (2002) 1270–1273.
[12] Catherine P. Whitby, Daniel Fornasiero, John Ralston, Structure of oil-in-water emulsions stabilised by silica and hydrophobised titania particles, J. Colloid Interface Sci. 342 (1) (2010) 205–209.
[13] S. Abend, N. Bonnke, U. Gutschner, G. Lagaly, Stabilization of emulsions by heterocoagulation of clay minerals and layered double hydroxides, Colloid Polym Sci. 276 (8) (1998) 730–737.
[14] A.A.D. Meirelles, A.L.R. Costa, R.L. Cunha, The stabilizing effect of cellulose crystals in O/W emulsions obtained by ultrasound process, Food Res. Int. 128 (2019), 108746.
[15] Yuh-Fun Maa, Chung Hsu, Liquid-liquid Emulsification by Rotor/stator homogenization, J. Control. Release 38 (2-3) (1996) 219–228.
[16] C Charcosset, I Limayem, H Fessi, The membrane emulsification process—a review, J. Chem. Technol. Biotechnol. 79 (3) (2004) 209–218.
[17] Shan He, Nikita Joseph, Shilun Feng, Matt Jellicoe, Colin L. Raston, Application of Microfluidic Technology in Food Processing, Food Funct. 11 (7) (2020) 5726–5737.
[18] C. Albert, M. Beladjine, N. Tsapis, E. Fattal, F. Agnely, N. Huang, Pickering emulsions: Preparation processes, key parameters governing their properties and potential for pharmaceutical applications, J. Control. Release 309 (2019) 302–332.
[19] A. Taha, E. Ahmed, A. Ismaiel, M. Ashokkumar, X. Xu, S. Pan, H. Hu, Ultrasonic emulsification: An overview on the preparation of different emulsifiers-stabilized emulsions, Trends Food Sci. Technol. 105 (2020) 363–377.
[20] Aureliano Agostinho Dias Meirelles, Ana Letícia Rodrigues Costa, Rosiane Lopes Cunha, Cellulose nanocrystals from ultrasound process stabilizing O/W Pickering emulsion, Int. J. Biol. Macromol. 158 (2020) 75–84.
[21] Y. Chen, V.N. Truong, X. Bu, G. Xie, A review of effects and applications of ultrasound in mineral flotation, Ultrason. Sonochem. 60 (2020), 104739.
[22] Tadao Nakashima, Masataka Shimizu, Masato Kukizaki, Particle control of emulsion by membrane emulsification and its applications, Adv. Drug Deliv. Rev. 45 (1) (2000) 47–56.
[23] S. Zhou, X. Wang, X. Bu, H. Shao, Y. Hu, M. Alheshibri, B. Li, C. Ni, Y. Peng, G. Xie, Effects of emulsified kerosene nanodroplets on the entrainment of gangue materials and selectivity index in aphanitic graphite flotation, Miner. Eng. 158 (2020), 106592.

[24] X. Wang, X. Bu, C. Ni, S. Zhou, X. Yang, J. Zhang, M. Alheshibri, Y. Peng, G. Xie, Effect of scrubbing medium's particle size on scrubbing flotation performance and mineralogical characteristics of microcrystalline graphite, Miner. Eng. 163 (2021), 106766.
[25] S. Zhou, X. Wang, X. Bu, M. Wang, B. An, H. Shao, C. Ni, Y. Peng, G. Xie, A novel flotation technique combining carrier flotation and cavitation bubbles to enhance separation efficiency of ultra-fine particles, Ultrason. Sonochem. 64 (2020), 105005.
[26] J.S. Laskowski, Chapter 5 Reagents, Elsevier, Amsterdam, Coal Flotation and Fine Coal Utilization, 2001, pp. 111–179.
[27] Èmir Tsabet, Louis Fradette, Effect of the properties of oil, particles, and water on the production of Pickering emulsions, Chem. Eng. Res. Des. 97 (2015) 9–17.
[28] B. Binks, S. Lumsdon, Catastrophic Inversion of Water-In-Oil Emulsions Stabilized by Hydrophobic Silica, Langmuir 16 (2000).
[29] P.T.L. Koh, F.P. Hao, L.K. Smith, T.T. Chau, W.J. Bruckard, The effect of particle shape and hydrophobicity in flotation, Int. J. Miner. Process. 93 (2) (2009) 128–134.
[30] Javad Saien, Mahdis Bahrami, Understanding the effect of different size silica nanoparticles and SDS surfactant mixtures on interfacial tension of n-hexane–water, J. Mol. Liq. 224 (2016) 158–164.
[31] H. Katepalli, V.T. John, A. Tripathi, A. Bose, Microstructure and rheology of particle stabilized emulsions: Effects of particle shape and inter-particle interactions, J. Colloid Interface Sci. 485 (2017) 11–17.
[32] M. Li, D. Wilkinson, K. Patchigolla, Comparison of particle size distributions measured using different techniques, Part. Sci. Technol. 23 (3) (2005) 265–284.
[33] Xuexia Wang, Shaoqi Zhou, Xiangning Bu, Chao Ni, Guangyuan Xie, Yaoli Peng, Investigation on interaction behavior between coarse and fine particles in the coal flotation using focused beam reflectance measurement (FBRM) and particle video microscope (PVM), Sep. Sci. Technol. 56 (8) (2021) 1418–1430.
[34] D.J. Law, A.J. Bale, S.E. Jones, Adaptation of focused beam reflectance measurement to in-situ particle sizing in estuaries and coastal waters, Mar. Geol. 140 (1-2) (1997) 47–59.
[35] J.M. Phillips, D.E. Walling, Calibration of a Par-Tec 200 laser back-scatter probe for in situ sizing of fluvial suspended sediment, Hydrol. Process. 12 (1998) 221.
[36] A.R. Heath, P.D. Fawell, P.A. Bahri, J.D. Swift, Estimating Average Particle Size by Focused Beam Reflectance Measurement (FBRM), Part. Part. Syst. Char. 19 (2) (2002) 84–95.
[37] Marie-Noëlle Pons, Kim Milferstedt, Eberhard Morgenroth, Modeling of chord length distributions, Chem. Eng. Sci. 61 (12) (2006) 3962–3973.
[38] Jophous Mugabi, Noriyuki Igura, Mitsuya Shimoda, Effect of Process Parameters on Oil-in-Water Emulsion Droplet Size and Distribution in Swirl Flow Membrane Emulsification, J. Chem. Eng. Jpn. 51 (3) (2018) 229–236.
[39] Ester Peris-García, Nikita Pankajkumar-Patel, María José Ruiz-Angel, Samuel Carda-Broch, María Celia García-Alvarez-Coque, Oil-In-Water Microemulsion Liquid Chromatography, Sep. Purif. Methods 49 (2) (2020) 89–111.
[40] Seid Mahdi Jafari, Elham Assadpoor, Yinghe He, Bhesh Bhandari, Re-coalescence of emulsion droplets during high-energy emulsification, Food Hydrocolloids 22 (7) (2008) 1191–1202.
[41] M. Stang, H. Schuchmann, H. Schubert, Emulsification in high-pressure homogenizers, Eng. Life Sci. 1 (4) (2001) 151–157.
[42] T.S.H. Leong, T.J. Wooster, S.E. Kentish, M. Ashokkumar, Minimising oil droplet size using ultrasonic emulsification, Ultrason. Sonochem. 16 (6) (2009) 721–727.
[43] S.G. Gaikwad, A.B. Pandit, Ultrasound emulsification: Effect of ultrasonic and physicochemical properties on dispersed phase volume and droplet size, Ultrason. Sonochem. 15 (4) (2008) 554–563.
[44] J.P. Canselier, H. Delmas, A.M. Wilhelm, B. Abismaïl, Ultrasound emulsification—an overview, J. Dispers Sci. Technol. 23 (1-3) (2002) 333–349.
[45] D. Gonzalez Ortiz, C. Pochat-Bohatier, J. Cambedouzou, M. Bechelany, P. Miele, Current trends in pickering emulsions: particle morphology and applications, Engineering 6 (4) (2020) 468–482.
[46] C. Gungoren, O. Ozdemir, X. Wang, S.G. Ozkan, J.D. Miller, Effect of ultrasound on bubble-particle interaction in quartz-amine flotation system, Ultrason. Sonochem. 52 (2019) 446–454.
[47] P. Blake, J. Ralston, Controlled methylation of quartz particles, Colloids Surf. 15 (1985) 101–118.